Hindawi
International Journal of Aerospace Engineering
Volume 2022, Article ID 2002423, 11 pages
https://doi.org/10.1155/2022/2002423

*Research Article*

# Optimization of Lateral Collision Risk of Aircraft Based on the Skid-Slip Event Model

**Hao Liu**,[1] **Daiwu Zhu**,[2] **Xiaofan Xie**,[3] **Jiuhao Chen**,[4] **and Xiaokang Liu**[5]

[1]*College of ATM, Civil Aviation Flight University of China, Guanghan, 618300 Sichuan, China*
[2]*Library, Civil Aviation Flight University of China, Guanghan, 618300 Sichuan, China*
[3]*Center for Teacher Development and Teaching Evaluation, Civil Aviation Flight University of China, Guanghan, 618300 Sichuan, China*
[4]*Academic Affairs Office, Civil Aviation Flight University of China, Guanghan, 618300 Sichuan, China*
[5]*School of Electronic Information, Zhongyuan University of Technology, Zhengzhou, 450007 Henan, China*

Correspondence should be addressed to Daiwu Zhu; 364890003@qq.com

Received 7 March 2022; Revised 11 June 2022; Accepted 7 July 2022; Published 15 July 2022

Academic Editor: Ti Chen



With the development of aircraft flow under the existing airspace capacity now, the shortage of airspace resources and flight delays have become significantly severe. Therefore, building a safe and efficient mathematical model from quantitative analysis and improving the scientificity of route planning and management are essential propositions for future research on new navigation systems. Based on the traditional event collision risk assessment model, the collision module is upgraded to an ellipsoid according to the performance of aircraft, integrating the boundary curvature optimization characteristics of the TSRRT (task-space rapidly-exploring random trees) algorithm. An aircraft event lateral conflict resolution model based on the TSRRT algorithm is proposed. Taking the A320 aircraft and 737-800 aircraft as experimental subjects, the corresponding collision coefficients are imported into software tools for the simulation and the Kalman filtering is combined to verify the smoothness of the front and rear boundary curvatures. The result proves that the event side collision risk of aircraft based on TSRRT is 15% of the traditional event model and the smooth curvature error is reduced by 80% due to the improvement. Therefore, the improved event model is practical and valuable, providing a theoretical basis for future track-based operations.

## 1. Introduction

With the rapid increase of aircraft flow, the existing air route network has become congested with limited airspace resources, which not only limits the increase in flight traffic but also causes much insecurity to flight [1]. Therefore, it is necessary to evaluate the collision risk of navigation from the scientific quantification perspective.

Domestic and foreign scholars have made many efforts to research the airway collision risk model. In 1966, Reich proposed the earliest collision risk model when evaluating the safety of separation standards for the North Atlantic route [2]. In 1984, Brooker applied the Reich model to the North Atlantic lateral collision risk study [3]. Brewer-Dougherty et al. [4] established a collision risk model of PBN (performance-based navigation) based on the Reich model in 2016. However, Kim and Hwang [5] conducted a practical comparison and analysis of the event model and Reich model in 2018, finding out that the event models are more inclusive and the models have apparent advantages in applying multiple integrations and superimposed factors. The event model (also known as the post-Reich model) was proposed by professor Brooker [6] of the United Kingdom in 2003, and a traditional cuboid collision template was established. In 2008, Xiaohao et al. [7] proposed using a cylindrical collision template instead of the traditional one to realize the function of risk assessment and calculating lateral intervals. In 2010, Wenjun et al. [8] used a spherical collision template to replace the traditional template to assess the safety of cross-route separation. In 2011, Yuling et al. [9] established a collision risk model based on a given arrival time interval for the flight at the same altitude and the same

direction with the help of the probability theory. In 2013, Zongping et al. [10] analyzed the approach risk of paired aircraft based on the accident tree analysis method and obtained the variation curve of the aircraft's longitudinal collision risk with relevant parameters through simulation calculation. It was assessed by Xingwu and Zhaoning [11] in 2015. In 2017, Jian [12] fully considered the speed error, navigation error, initial safe distance, and other factors of the two aircraft during the paired approach of the short-distance parallel runway to establish a paired approach collision risk assessment model; in 2018, Xinsheng and Zhi [13] studied the flight interval and conflict relief threshold under the influence of multiple random factors. In 2019, Shuo [14] used a cylinder-rectangular collision temlate to study the collision probability of UAVs. In 2021, Xie et al. [15] comprehensively considered the influence of aircraft yaw and established a paired approach longitudinal collision risk assessment model for the longitudinal separation calculation of aircraft at each stage. However, none of the above-mentioned event collision models can reflect the speed vector changes in the aircraft space and the aircraft sideslip curvature cannot be described. More importantly, due to the aircraft's pitch angle limitation, the aircraft will generally change the height to prevent a collision when the two aircraft are approaching, so the space formed by the aircraft's deflection around the lateral axis of the wing is not a cuboid or sphere, but a cylinder close to it. Therefore, a skid-slip event lateral conflict resolution model is proposed to analyze and study the lateral risk of the air routes.

## 2. Event Lateral Model Construction and Improvement

*2.1. Event Model Construction.* The event model evaluates the collision risk of adjacent-tracking aircraft (labeled AIR-A and AIR-B) with a lateral separation of $S$. AIR-A is used as the center point to simulate a cylinder with a radius of $D$ ($\lambda_x$ and $\lambda_y$ representing the horizontal and vertical lengths of the aircraft, respectively. It is assumed that the wingspan and the length of the aircraft are equal, that is, $\lambda_x = \lambda_y$, both expressed in terms of aircraft length $D$) and a height of $2\lambda_z$ (the height of the aircraft is represented by $\lambda_z$, taking the center point of the aircraft as the center of the cylinder, and the height of the cylinder is $2\lambda_z$) [16]. AIR-B is used as the origin to simulate a plane with no thickness on the $x$–$z$-axes. When the spacing piece of AIR-B is in contact with the cylinder of AIR-A, that is, AIR-A and AIR-B are in an absolute collision, the schematic diagram is described in Figure 1 as follows.

For AIR-A and AIR-B, $T_C$ is used to represent the voyage time and the number of collisions per unit time of voyage can be expressed as follows:

$$\mathrm{CR} = 2\mathrm{NP} \times \mathrm{HOR}(T_C) \times P_z(S_z) \times \left(1 + \frac{\pi D|z|}{4\lambda_z V_{\mathrm{rel}}^C}\right), \quad (1)$$

where NP is the number of aircraft logs per hour and HOR $(T_C)$ is the probability that AIR-A and AIR-B overlap horizontally. $P_z(S_z)$ is the probability that AIR-A and AIR-B overlap vertically when the horizontal overlap occurs, which generally takes a fixed value of $6.6 \times 10^{-6}$. $|z|$ is the average vertical relative speed. $V_{\mathrm{rel}}^C$ is the average horizontal relative speed. When studying the lateral risk model of adjacent trajectories, the voyage report period is set to $T$ hours, the number of planes is set to $\mathrm{NP} = 1/T$ when calculating the lateral interval, and it is assumed that the two planes fly at the cruise level. When the lateral interval is unknown, it can be replaced by $P_z(0)$ and the number of collisions per hour on the same track can be expressed as follows:

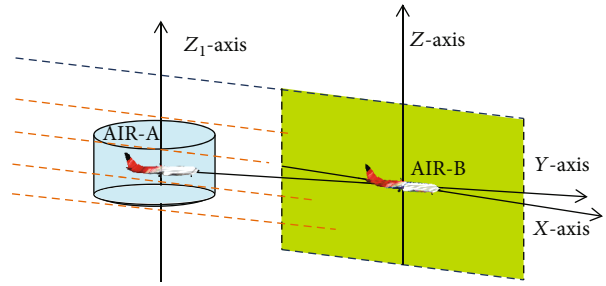


Figure 1: The collision box laterally traverses the spacer layer.

$$\mathrm{CR}(T) = \frac{2}{T} \times \mathrm{HOR}(T + \tau) \times P_z(0) \times \left(1 + \frac{\pi D|z|}{4\lambda_z V_{\mathrm{rel}}^C}\right). \quad (2)$$

$\tau$ is the communication and controller intervention buffer value based on the CPDLC data link (controller and pilot data link communication); the horizontal overlap probability $\mathrm{HOR}(T + \tau)$ is based on the vertical overlap probability and lateral overlap at $t = T + \tau$. So, the probability can be expressed as follows:

$$\begin{aligned} &\mathrm{HOR}(T + t) = \mathrm{LOP} \times P_y(0), \\ &P_{(T+t)} = \mathrm{LOP} \times P_y(0) \times P_z(0) \times \left(1 + \frac{\pi D|z|}{4\lambda_z V_{\mathrm{rel}}^C}\right), \end{aligned} \quad (3)$$

where LOP is the probability of the longitudinal overlap and $P_y(0)$ is the probability of the lateral overlap of 2 aircraft on adjacent levels of the track.

*2.2. Collision Ratio R*

*2.2.1. Conavigation Collision Relationship Ratio R.* Figure 2 shows the movement of the crash box laterally and longitudinally across the spacer in the case of codirectional flight. If a collision occurs, the aircraft point $B$ must be within the line segment JK. When the aircraft point $B$ is outside the line segment JK on the line segment IL, that is, on the line segment IJ and the line segment KL, there will be no collision. In the event model, since the collision box is the cuboid shown in the figure, during the entire process of crossing the spacer, as long as point $B$ is on the line segment IL, a collision may occur. When flying on the same heading, the collision box laterally traverses the spacer and moves in the lateral and longitudinal directions. According to the geometric principles, point $B$ collides in the line segment JK.

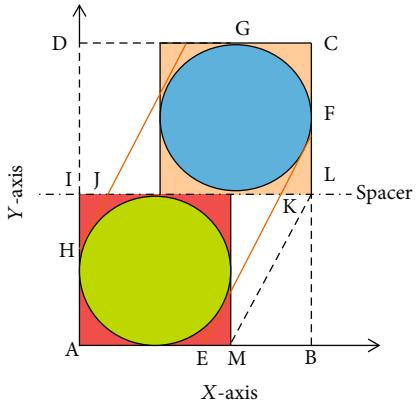


Figure 2: Collision geometry diagram in the same direction.

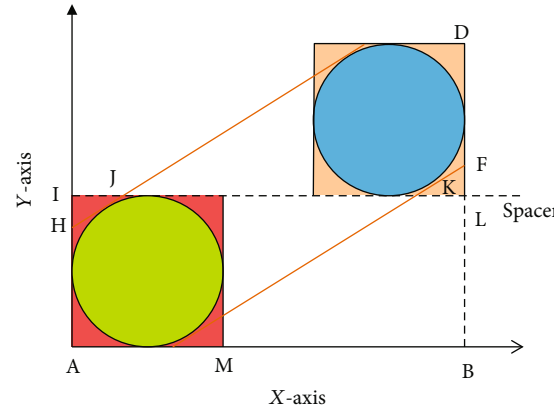


Figure 3: Reverse navigation collision geometry diagram.

Otherwise, it does not crash. According to the characteristics of the event model, it can be described that when point $B$ is on the line segment IL, AIR-A and AIR-B will hit each other.

Assuming that $B$ is relatively stationary, considering the collision probability relationship ratio $R(S)$ from a geometric point of view, the longitudinal movement distance of AIR-A is BM, which can be expressed as follows:

$$\begin{aligned} R(S) &= \frac{\mathrm{JK}}{\mathrm{IL}}, \\ \mathrm{BM} &= \frac{2D}{V} \times U. \end{aligned} \tag{4}$$

$U$, $V$, and $W$ are the relative velocities of A-AIR through the AIR-B spacer in the longitudinal, lateral, and vertical directions when sailing in the same direction [17]. At the same time, they can float in the same direction according to the geometry and the event model motion principle. The collision probability relationship ratio is as follows:

$$R(S) = \frac{U + 2V}{2U + 2V}. \tag{5}$$

*2.2.2. Reverse Navigation Collision Relationship Ratio R1.* The longitudinal relative speed of AIR-A and AIR-B when cruising in the reverse direction is $2U_{\mathrm{at}}$. It is assumed that the relative speed change value in the lateral and vertical movement is 0, that is, the time for the reverse sailing to pass through the interval is equal to the time in the same direction. The schematic diagram of the collision cylinder passing through the spacing piece when traveling in the reverse direction is shown in Figure 3.

According to Figure 3, considering the geometric ratio relationship, the length of MB and IL can be expressed as follows:

$$\begin{aligned} \mathrm{MB} &= \frac{2D}{V} \times 2U_{\mathrm{at}}, \\ \mathrm{IL} &= 2D + \frac{2D}{V} \times 2U_{\mathrm{at}}. \end{aligned} \tag{6}$$

Since IL is much larger than KL, the approximate length of the KL line segment is $D$ and the collision probability relationship between AIR-A and AIR-B when sailing in the reverse direction is as follows:

$$R(O) = \frac{2U_{\mathrm{at}}}{2U_{\mathrm{at}} + V}. \tag{7}$$

*2.3. Integration of Skid-Slip Event Model.* Since the TSRRT algorithm will integrate kinematic model constraints into the route planning, the curvature of the overall planning can be optimized so that the path curvature can meet the need for parameter continuity [18]. Also, it is easy to solve the length of the line segment and rough value of KL in the same direction and reverse navigation collision geometric model. Because the TSRRT algorithm adopts the Dubins curve, it can effectively reduce the convergence time of risk assessment when the sailing demands are met.

The motion model of the Dubins curve only allows the moving body to move forward and not to return, and the line can connect the shortest path in a two-dimension surface under the circumstances that the curve is satisfied with path constraints. This article uses RSL to represent the shortest path connecting the two control points of $P_0$ and $P_1$, where the radius in the curve circle is the radius of the bottom surface of the cylinder. That is, $R$ and $D$ are equal and the corresponding RSL diagram is shown in Figure 4 as follows.

The TSRRT firstly samples and marks the nodes in the areas prone to lateral overlap, integrating the heuristic function to calculate the value of the central point of the lateral adjacent overlap area. Let $G$ be the combination of adjacent nodes with the smallest total value of the current risk.

$$G = \arg\min\left(H(S)\right). \tag{8}$$

$H(S)$ is the substitute value of adjacent overlapping risk areas. Let $H(Q)$ be the total risk calculation cost from the initial risk overlapping point to the current period, and

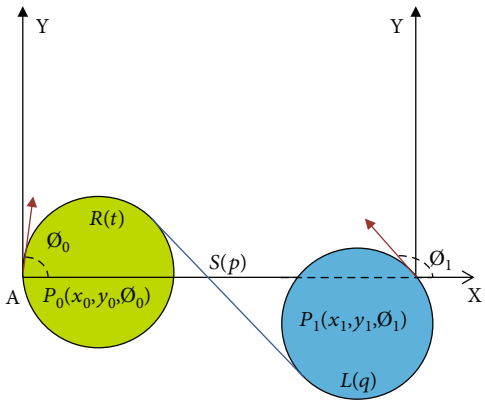


Figure 4: Schematic diagram of RSL.

$H(G)$ is the estimated value at risk from the current period to the target point.

$$H(Q) = \sum_{i=2}^{n} L_{bci},$$
$$L_{bci} = \frac{2L_c + (n-1)L_p}{n+1}. \tag{9}$$

$L_{bci}$ is the approximate length of the $i_{\text{th}}$ adjacent point and the Bezier curve, and $n$ is the Bezier order, which is the side collision surface of A-AIR and B-AIR running in the same or reverse direction.

## 3. Kalman Filter Error Model Based on RNP

The fusion of the TSRRT algorithm and the event model could reduce the convergence time and increase the accuracy of KL under geometric analysis. However, it cannot meet the requirements of free navigation in the ICAO.DOC9750 global navigation plan [19]. The yaw probability-based Kalman filtering is introduced to evaluate the multifactor superimposition effect on the collision model so that the practicability, accuracy, and reproducibility of the event lateral conflict model can be improved in future navigation systems [20, 21]. The total yaw error TSE (total system error) under lateral confliction error is generally composed of NSE (navigation system error), PDE (path definition error), and FTE (flight technical error). The RNP (required navigation performance) program can be selected as a benchmark when measuring the error probability under lateral conflict. RNPN can be described as the aircraft's actual position being within ±95% of the total flight time. In other words, it is safe in the range of $N$ NM [22, 23] and there will be no risk of collision, as shown in Figure 5.

The Kalman filter is based on the theory of the state equation and motion vector equation of the moving aircraft, and the least mean square error is used as the reference to estimate the system state [24]. Therefore, the minimum mean square error threshold can be selected to correspond to the RNP regulations. The filter error is used to measure the event's lateral direction, the applicability, and the rationality of the conflict model. The Kalman system equation is as follows:

$$X(n) = A(n|n-1)X(n-1) + B(n|n-1)\omega(n-1),$$
$$Z(n) = H(n)X(n) + v(n), \tag{10}$$

where $X(n)$ is the state vector, which represents the value of the motion vector at time $n$. $A(n \mid n-1)$ is the state transition matrix used to describe the motion of the target object. $B(n \mid n-1)$ is the interference transition matrix. $\omega(n)$ represents the system noise of the motion model. $Z(n)$ represents the observation vector, describing the observation value at time $n$. $H(n)$ is the observation matrix; $v(n)$ is the motion observation noise generated during the estimation process, and $\omega(n)$ and $v(n)$ are independent of each other. Its statistical characteristics are as follows:

$$E\left[\omega(n)\omega^T(i)\right] = \begin{cases} Q(n), & i = n, \\ 0, & i \neq n, \end{cases}$$
$$E\left[v(n)v^T(i)\right] = \begin{cases} R(n), & i = n, \\ 0, & i \neq n, \end{cases} \tag{11}$$

$$E\left[w(n)v^T(i)\right] = 0. \tag{12}$$

At the same time, the Kalman equation of motion can be divided into the time update equation and the observation update equation, here named

$$X(n|n-1) = A(n|n-1)X(n-1|n-1),$$

$$P(n|n-1) = A(n|n-1)P(n-1|n-1)\cdot A^T(n|n-1) + B(n|n-1)Q(n-1)\cdot B^T(n|n-1),$$

$$X(n|n) = X(n|n-1) + K(n)[Z(n) - H(n)X(n|n-1)],$$

$$K(n) = P(n|n-1)H^T(n)\left[H(n)\cdot P(n|n-1)H^T(n) + R(n)\right]^{-1},$$

$$P(n|n) = [I - K(n)H(n)]P(n|n-1), \tag{13}$$

where $Q(n)$ is the symmetric nonnegative definite azimuth matrix of the system noise $\omega(n)$. $R(n)$ is the symmetric positive definite variance matrix of the observation noise $v(n)$. $P(n \mid n)$ is the error variance matrix. $K(n)$ is the filter gain matrix [25].

According to the definition of the abovementioned system equations and the physical relationship of the

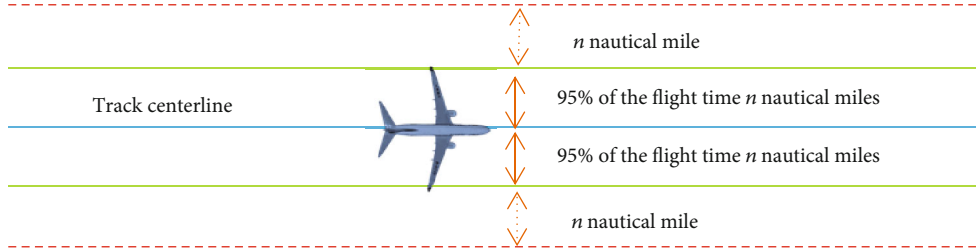


Figure 5: Schematic diagram of the RNP procedure.

parameters, the state transition matrix $A(n \mid n-1)$ and the observation matrix $H(n)$ can be obtained.

$$A(n|n-1) = \begin{bmatrix} 1 & 0 & T & 0 & 0 & \frac{T^2}{2} & 0 \\ 0 & 1 & 0 & T & 0 & \frac{T^2}{2} & \\ 0 & 0 & 1 & 0 & T & 0 & \\ 0 & 0 & 0 & 1 & 0 & T & \\ 0 & 0 & 0 & 0 & 1 & 0 & \\ 0 & 0 & 0 & 0 & 0 & 1 & \end{bmatrix}, \quad (14)$$

$$H(n) = \begin{bmatrix} 1 & 0 & 0 & 0 & 0 & 0 \\ 0 & 1 & 0 & 0 & 0 & 0 \end{bmatrix}. \quad (15)$$

## 4. Simulation Calculations

To test the effectiveness and efficiency of the aircraft event lateral conflict resolution model based on TSRRT, an Intel Core i7 processor is selected as the hardware operating environment with a 16 GB memory capacity.

The wingspan, fuselage, and fuselage heights of the A320 aircraft are 34.1 m, 37.6 m, and 11.8 m, respectively, $R_1 =$ max (34.1, 37.6) (unit: m). The wingspan, fuselage, and fuselage height of the B737-800 aircraft are 35.79 m, 39.47 m, and 12.57 m, respectively, $R_2 =$ max (35.79 m, 39.47 m). The ADS-B-based position and time information of the A320 and B737-800 aircraft are selected as the primary simulation data in the experiment. Some of the position and time data are shown in Tables 1 and 2.

According to the requirements of ≪introduction to safety assessment of flight intervals≫ [26], considering the maximum risk of lateral collision, the lateral relative velocity $v$ is set to 6.44 m/s and the longitudinal relative velocity $u$ is set to 514 m/s, vertical relative velocity $|z| = w = 0.78$ m/s, $D_1 = 37.6$ m, $D_2 = 39.47$ m, $\lambda_{z1} = 11.80$ m, and $\lambda_{z2} = 12.57$ m. According to the literature [27–29], the lateral overlap probability is $P_y(0) = 0.0432$, the longitudinal overlap probability LOP $= P_x(0) = 0.0432$, the vertical overlap probability $P_z(S_z) = 6.6 \times 10^{-6}$, the longitudinal proximity rate $E(0)$ is 0.01, $\tau = 4$ min, the longitudinal interval $W$ of the aircraft is 10 km, the target offset rate $P_{\text{goal}} = 0.1$, the maximum curvature $k_{\max} = 0.05$, the maximum sideslip steering angle $\gamma = 0.4$ pi, and the sampling step length $d = 10$ km, as shown in Table 3.

The event parameters set in Table 3 are brought into the lateral conflict model, and the collision risk values of the original cylindrical event lateral conflict model and the improved skid-slip event lateral conflict model are obtained; the obtained calculation result (retaining two decimal places) is shown in Table 4.

As the safety target level specified in ICAO Annex 6 11th Edition [30] is $5 \times 10^{-9}$, the collision probabilities of the traditional event model and the improved skid-slip event model are $1.12 \times 10^{-10}$ and $7.48 \times 10^{-10}$, respectively, when choosing the 1st combination (A320), which meets the target level specified by ICAO, and the optimized event collision probability becomes 15% ($1.12 \times 10^{-10}/7.48 \times 10^{-10}$). Similarly, the collision probabilities of the traditional event model and the improved skid-slip event model are $1.12 \times 10^{-10}$ and $7.43 \times 10^{-10}$ when using the B737-800 combination. The collision probability of the B737-800 combination model before and after the improvement is less than $5 \times 10^{-9}$, and the optimized event collision probability becomes 15% ($1.12 \times 10^{-10}/7.43 \times 10^{-10}$) of the traditional event model.

## 5. Main Factor Analysis and Improved Model Test

*5.1. Analysis of Main Factors.* It can be seen in Tables 3 and 4 that the collision risk probability is mainly affected by the flight time and the speed error. The following mainly analyzes the collision risk from the two aspects of the flight time change and the speed error parameter. Let the airplane speed $v = 460$ kt, the value of airplane speed error parameter $\sigma = 7.0$, and the time interval be 5 min. The safety target-level risk time specified in ICAO Annex 6 is $5 \times 10^{-9}$ times/flight hour [30], and the logarithm based on 10 is lg $(5 \times 10^{-9}) = -8.301$, which is different for different RNP specifications. The changing trend of collision risk is shown in Figure 6.

It can be seen in Figure 6 that the risk of collision and the collision specifications of different navigation sources also differ significantly as the flight time increases. Taking RNP4 as an example, the collision risk changes from $10^{-18}$ to $10^{-9}$ overtime. The collision risk change interval of RNP10 is $[10^{-11}, 11^{-9}]$ because the navigation error parameter value of RNP10 is 5.1, which is 2.5 in the case of RNP4. The difference in navigation specifications makes the flight error significantly increase. When the flight time is 90 minutes, the collision risk of RNP10 is $5.3 \times 10^{-9}$ (which is

Table 1: Part of the A320 passenger location and time information table based on ADS-B.

| Serial numbers | Times | Latitudes | Longitudes | Heading | m/s |
|---|---|---|---|---|---|
| 01 | 07:47:16 | 29.3472 | 118.3324 | 120° | 213.6 |
| 02 | 07:48:10 | 29.3037 | 118.2116 | 120° | 225.2 |
| 03 | 07:49:10 | 29.2551 | 118.0766 | 120° | 233.3 |
| 04 | 07:49:43 | 29.2293 | 118.0037 | 120° | 232.7 |
| | | | … | | |
| 20 | 08:02:15 | 28.6792 | 116.4662 | 120° | 226.6 |
| 21 | 08:02:45 | 28.6568 | 116.4034 | 120° | 231.7 |
| 22 | 08:03:15 | 28.6332 | 116.3378 | 120° | 233.3 |
| | | | … | | |

Table 2: Part of B737-800 location time information table based on ADS-B.

| Serial numbers | Times | Latitudes | Longitudes | Heading | m/s |
|---|---|---|---|---|---|
| 01 | 07:47:16 | 28.4138 | 118.4220 | 143° | 226.7 |
| 02 | 07:48:10 | 28.4060 | 118.3654 | 143° | 230.6 |
| 03 | 07:49:10 | 28.3941 | 118.2832 | 143° | 234.2 |
| 04 | 07:49:43 | 28.3838 | 118.2149 | 143° | 232.5 |
| | | | … | | |
| 20 | 08:02:15 | 28.3740 | 116.1492 | 143° | 231.9 |
| 21 | 08:02:45 | 28.3623 | 116.0717 | 143° | 232.5 |
| 22 | 08:03:15 | 28.3515 | 116.0001 | 143° | 232.5 |
| | | | … | | |

Table 3: Event lateral conflict model parameter setting table based on TSRRT.

| Parameters | Numbers | Parameters | Numbers |
|---|---|---|---|
| $u$ (m·s$^{-1}$) | 514 | $D_1$ (m) | 37.60 |
| $v$ (m·s$^{-1}$) | 6.44 | $D_2$ (m) | 39.47 |
| $w$ (m·s$^{-1}$) | 0.78 | $\lambda_{z1}$ (m) | 11.80 |
| $d$ (km) | 10 | $\lambda_{z2}$ (m) | 12.57 |
| $P_x(0)$ | 0.0432 | $P_y(0)$ | 0.0432 |
| $P_z(S_z)$ | $6.6 \times 10^{-6}$ | $E(0)$ | 0.01 |
| $\tau$ (min) | 4 | $W$ (km) | 10 |
| $P_{\text{goal}}$ | 0.1 | $k_{\max}$ | 0.05 |
| $\gamma$ | 0.4 pi | | |

Table 4: Collision risk assessment results.

| Collision combination types | The original cylinder event model | Improved event model based on TSRRT | Safety target level |
|---|---|---|---|
| Combination 1 (A320) | $1.12 \times 10^{-10}$ | $7.48 \times 10^{-10}$ | $5 \times 10^{-9}$ |
| Combination 2 (B738) | $1.12 \times 10^{-10}$ | $7.43 \times 10^{-10}$ | $5 \times 10^{-9}$ |

more than the $5.0 \times 10^{-9}$), which cannot meet the given safety target level of ICAO. The requirements can be met only by shortening the flight time or increasing the time interval. As shown in Figure 7, the number of collisions under different navigation specifications increases when the speed error parameter value $\sigma$ changes. When $\sigma = 2$, the number of collisions of RNP4, RNP5, and RNP10 are −27.1, −22.0, and −11.6, respectively. Under the same speed error $\sigma$, RNP10 safety factor > RNP5 safety factor > RNP4 safety factor, and as the speed error parameter value increases, the collision risk changes decrease.

*5.2. Improved Model Checking.* When the Kalman filter is used to test the yaw probability model, the sampling period

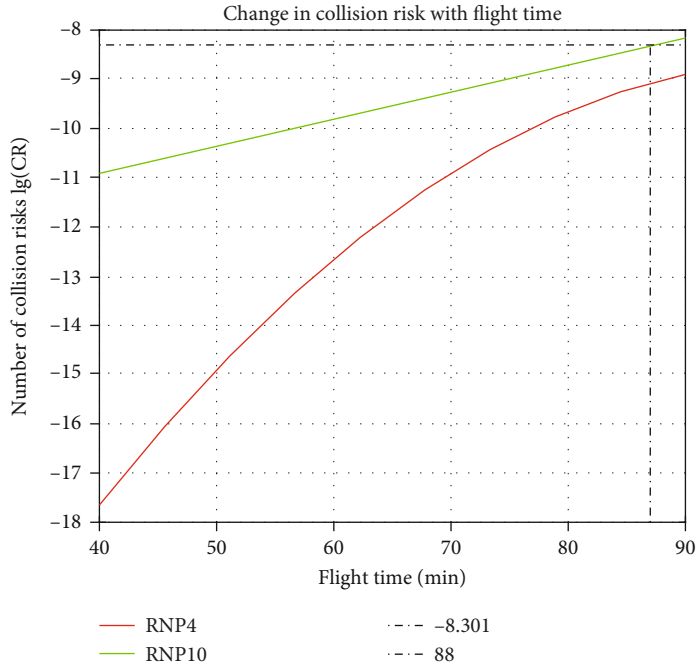


Figure 6: Collision risk changes with the flight time.

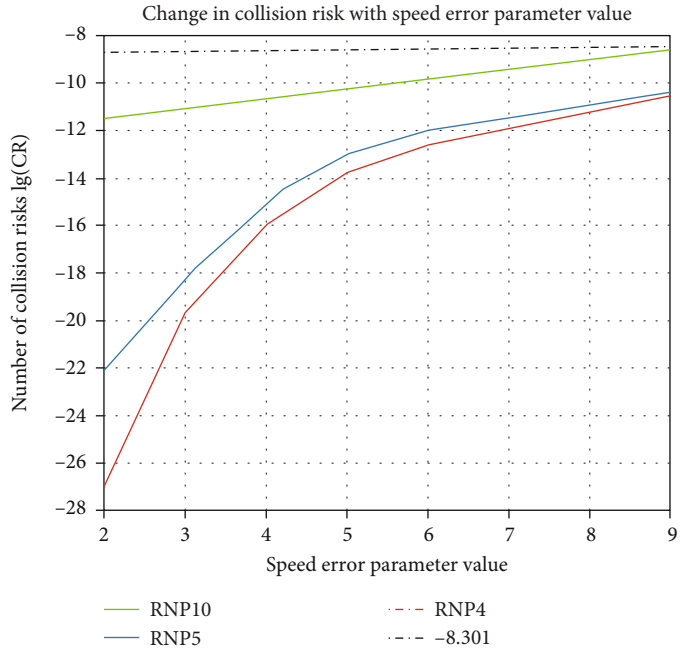


Figure 7: Collision risk changes with navigation speed error.

is controlled within the interval of $35 \pm 5S$ and the observed noise value $R(n) = 0.01 \times I_{4\times4}$, $Q(n) = I_{1\times1}$, $P(0 \mid 0) = 8 \times I_{6\times6}$, the system noise parameter is $B(n|n\text{-}1) = 0.01 \times I_{6\times1}$, with equations (12)–(15), and the corresponding motion filter is shown in Figures 8 and 9,

According to the requirements of ICAO.DOC4444《air traffic management》 [31], the width of the route is 20 km, with 10 km on both sides of the centerline. When conditions restrict a specific route section, the width can be reduced but it should not be less than 8 km. The maximum distance of ADS-B pulse yaw in Figure 8 is 10 km, and the minimum is 4 km, so it can well meet the navigation requirements of ICAO. At the same time, the curve clusters are analyzed. The comparison of $P(n \mid n)$ of the central mainline to the right benchmark mainly fluctuates in the range of [−10,0], and the $P(n \mid n)$ comparison benchmarks of a small part of

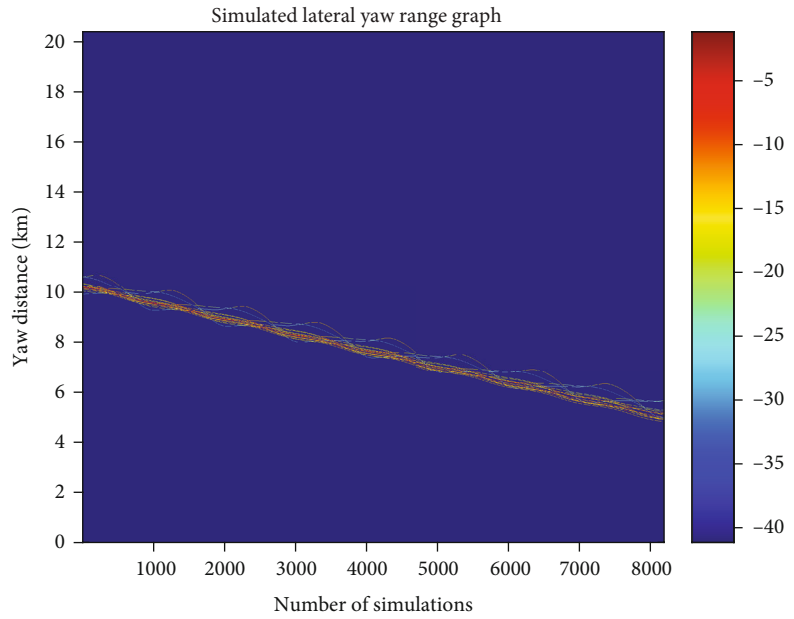


Figure 8: The simulated yaw curve under the ADS-B pulse pair.

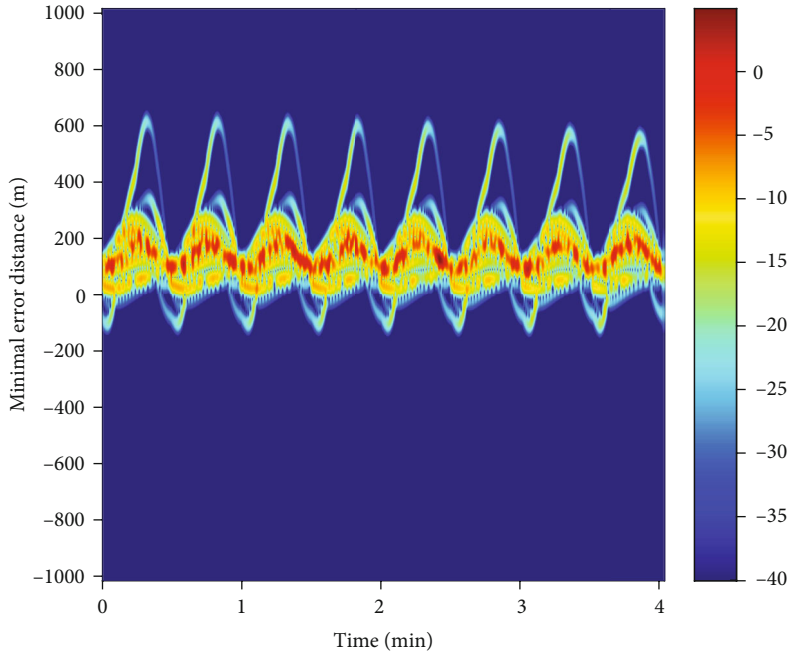


Figure 9: Research on track smoothness based on the Kalman filter.

the edge curves are mainly in [−30, −25] (unit: m) range. It can also meet the requirements for CNS in ICAO Annex 6 [28]. At the same time, the aircraft lateral slip analysis is performed on the filtering of Figure 9. The minimum error distance mainly fluctuates in the interval of [200,300] (unit: m). Because the general route width is ±20 km, the relative route slip ratio during the sailing time is 0.01. The RNP is selected as the flight navigation specification in the air route. The required coefficient of the sideslip time is ≤0.05, and the minimum sideslip coefficient of the RNP is 0.05. The filter sideslip rate of Figure 9 is much less than 0.05. The test shows that the event lateral conflict model based on TSRRT is effective and reasonable. It can meet the needs of TBO (trajectory-based operation).

$$f(x) \sim N\left(\mu(x), k\left(x, x'\right)\right), \tag{16}$$

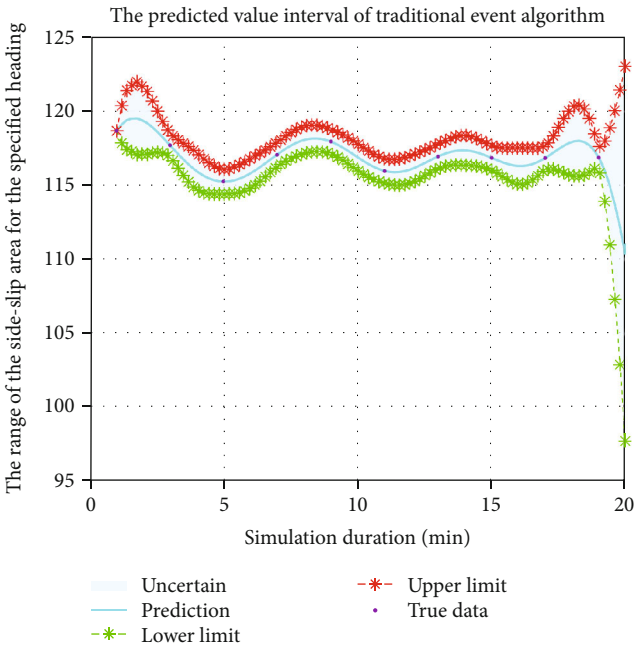


Figure 10: Prediction points and prediction intervals based on the traditional event model.

$$k\left(x, x'\right) = \theta_0^2 \exp\left(-\frac{\left(x - x'\right)^2}{2\theta_1^2}\right) + \sigma^2 \delta_{ij}, \tag{17}$$

where $\mu(x)$ is the mean function; $k(x, x')$ is the covariance function; $\delta_{ij}$ is the Dirac function; when $i = j$, $\delta_{ij} = 1$; otherwise, it is 0.

At the same time, because the Kalman filter is based on the state equation and motion vector equation of the moving aircraft, the minimum mean square error is used as the basis to estimate the system state [24]. Gaussian process regression (GPR) includes the noise variance test and Gaussian process prior. The maximum likelihood function in the Gaussian process regression is selected as the test standard. The lateral offset margin can be estimated while predicting the accurate point of the route to provide higher safety and reliability for future free navigation. Putting the parameters in Table 3 into formula (17) ($\theta_0 = \theta_1 = 0.3$), the predicted values and intervals of its traditional event model and skid-slip event model can be obtained, as shown in Figures 10 and 11.

As shown in Figure 10, in the traditional event model, the upper limit of the interval is 122° and the lower limit of the interval is 115°; that is, the prediction interval is [115°,122°], the maximum difference of the prediction interval is 7°, and the interval boundary is volatile. It is not convenient for maneuvering in the main and auxiliary sections of the RNP route. In the improved event model of Figure 11, the upper limit of the interval is 119° and the lower limit of the interval is 116°; that is, the prediction interval is [116°,119°] and the maximum difference is 3°, compared with before the improvement, the sideslip angle is reduced by 4°. In addition, the interval boundary line is relatively smooth, which is more in line with RNP route specifications and operation well.

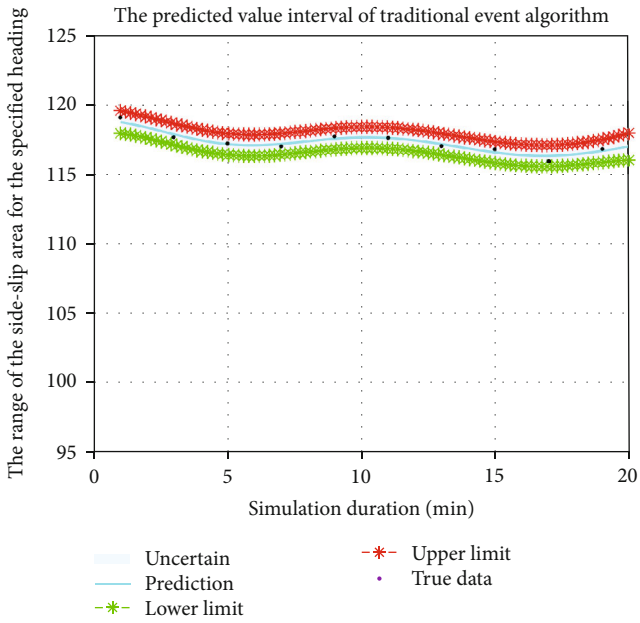


Figure 11: Forecast points and forecast intervals based on the improved event model.

## 6. Conclusion

This paper selects the event lateral conflict resolution model based on TSRRT and takes the combination of A320 aircraft and B737-800 aircraft as the experimental subject. The calculation shows that the side collision probability of the improved event model is 15% of the collision probability of the traditional event model and the dynamic sideslip curvature error per unit time is reduced by 80%, indicating that the improved event model is effective and reasonable.

Through the analysis of the flight time change parameters and speed error parameter values in the event model, the collision risk increases with the parameter value. The collision risk decreases with the RNP error change within a given time, and it will be free to sail in the future. The performance of the CNS system can be improved to shorten the flight time or appropriately increase the safety margin.

Because the Kalman filter can analyze errors and improve the prediction accuracy, this article uses ICAO.DOC4444 as a guide to calculate the data obtained by the ADS-B query response pulse using the Kalman filter to verify that the improved event model is efficient.

The research object of this paper is only studying the lateral conflict model to satisfy the 4D trajectory operation in ASBU (aviation system block upgrade). It can be studied from the longitudinal, vertical, and mixed directions in the future to obtain a more practical conflict resolution model.

## Data Availability

The numerical simulation data used to support the findings of this study are included in the article.

## Conflicts of Interest

The authors declare that they have no conflicts of interest.

## Acknowledgments

This work was sponsored in part by the "Visual Flight Programming and Approval Guidelines Project of RNAV Procedures" (no. 14002600100015J013), "Special Guidance Found of Building World-Class Universities (Disciplines) and Characteristic Development" (no. D202103), and "Innovation and Entrepreneurship Training Program for College Students of Sichuan Province" (no. 202210624005).We are grateful for the support of these funds.

## References

[1] Q. Yuling, *Research on Air Traffic Collision Risk Models*, Nanjing University of Aeronautics and Astronautics, Nanjing, 2012.

[2] P. Reich, "Analysis of long-range air traffic systems: separation standards—III," *Journal of Navigation*, vol. 19, no. 3, pp. 331–347, 1966.

[3] P. Brooker, "Aircraft collision risk in the North Atlantic region," *Journal of the Operational Research Society*, vol. 35, no. 8, pp. 695–703, 1984.

[4] T. Brewer-Dougherty, B. Colamosca, C. Gerhardt-Falk et al., "Collision risk modeling in the Northern Pacific airspace under separation reduction and improvements in navigational performance," *Air Traffic Control Quarterly*, vol. 14, no. 4, pp. 257–282, 2006.

[5] K. Kim and I. Hwang, "Intent-based detection and characterization of aircraft maneuvers in en route airspace," *Journal of Aerospace Information Systems*, vol. 15, no. 2, pp. 72–91, 2018.

[6] P. Brooker, "Lateral collision risk in air traffic track systems: a 'post-Reich' event model," *Journal of Navigation*, vol. 56, no. 3, pp. 399–409, 2003.

[7] X. Xiaohao, W. Zhenyu, and Z. Hongsheng, "Event-based side collision risk improvement model," *Journal of the Civil Aviation University of China*, vol. 3, pp. 1–4, 2008.

[8] Y. Wenjun, L. Tingting, and L. Jimin, "Research on the safety assessment of cross-airway flights interval," *Aeronautical Computing Technology*, vol. 40, no. 1, pp. 11–15, 2010.

[9] Q. Yuling, H. Songchen, and Z. Ming, "Collision risk model of turning airway," *Transportation Engineering*, vol. 11, no. 3, pp. 88–92, 2011.

[10] L. Zongping, L. Yanfei, and Z. Zhaoning, "Research on collision risk for paired approach based on fault tree analysis method," *Science Technology and Industry*, vol. 13, no. 4, pp. 130–134, 2013.

[11] C. Xingwu and Z. Zhaoning, "Cross route collision risk assessment based on event improved model," *Journal of China Civil Aviation University*, vol. 33, no. 3, pp. 1–4, 2015.

[12] W. Jian, *Study on the Risk of Paired Approach Collision in Close Parallel Runway*, Civil Aviation University of China, Tianjin, 2017.

[13] Y. Xinsheng and R. Zhi, "Study on flight interval assessment and conflict resolution threshold under the influence of multiple random factors," *Journal of Safety and Environment*, vol. 18, no. 1, pp. 1–4, 2018.

[14] Y. Shuo, *Research on the Modeling Method of Large-Scale UAV Collision Models*, Hebei University of Science and Technology, Shijiazhuang, 2019.

[15] C. Xie, X. Liang, and F. Lu, "Based on thestatistical distribution, the risk assessment of paired approach longitudinal collisions in close parallel runways," *Science Technology and Engineering.*, vol. 21, no. 10, pp. 4284–4288, 2021.

[16] D. A. Hsu, "The evaluation of aircraft collision probabilities at intersecting air routes," *Journal of Navigation*, vol. 34, no. 1, pp. 78–102, 1981.

[17] W. Pingan, "Risk prediction of collision between military aviation domain and civil aviation route in the lateral interval," *Firepower and Command Control*, vol. 44, no. 1, pp. 87–92, 2019.

[18] K. Yang and S. Sukkarieh, "An analytical continuous-curvature path-smoothing algorithm," *IEEE Transactions on Robotics*, vol. 26, no. 3, pp. 561–568, 2010.

[19] International Civil Aviation Organization (ICAO), *Doc9750-AN/963-2016-2030 Global Air Navigation Plan (FIFTH EDITION)*, ICAO, Montréal,Canada, 2016.

[20] L. Ma, Y. Tian, S. Yang, C. Xu, and A. Hao, "A scheme of sustainable trajectory optimization for aircraft cruise based on comprehensive social benefit," *Discrete Dynamics in Nature and Society*, vol. 2021, Article ID 7629203, 15 pages, 2021.

[21] Y. Zou, H. Zhang, G. Zhong, H. Liu, and D. Feng, "Collision probability estimation for small unmanned aircraft systems," *Reliability Engineering & System Safety*, vol. 213, p. 107619, 2021.

[22] Z. Daiwu and H. Guangqin, *Visual and Instrument Flight Program Designs*, Southwest Jiaotong University Press, Chengdu, 3rd edition, 2016.

[23] International Civil Aviation Organization (ICAO), *Doc 8168-OPS/611-Volume II Procedure for Air Navigation Services-Aircraft Operation (Volume II)Construction of Visual and Instrumental Flight Procedures (Sixth Edition)*, ICAO, Montréal, Canada, 2014.

[24] Z. Shuibing, T. Cheng, L. Shan, and W. Dejun, "Ship trajectory prediction based on improved Kalman filter in the controlled river," *Computer Applications*, vol. 32, no. 11, pp. 3247–3250, 2012.

[25] Y. Yang, Z. Suqin, and D. Guilan, "Integrated navigation technology based on federated Kalman filtering on the Beidou double star positioning system," *Computer Science*, vol. 3, pp. 110–113, 2007.

[26] Z. Zhaoning, W. Lili, and L. Dongbin, *Introduction to Flight Separation Safety Assessment*, Science Press, Beijing, 2009.

[27] Z. Xiaoyan and P. Weijun, "Safety assessment of vertical separation in RVSM airspace," *Aeronautical Computing Technology*, vol. 39, no. 5, pp. 5–8, 2009.

[28] K. I. Tenekedjiev, N. D. Nikolova, and K. Kolev, "Applications of Monte Carlo simulation in modelling of biochemical processes," in *Applications of Monte Carlo Methods in Biology, Medicine and Other Fields of Science*, C. J. Mode, Ed., InTech, Rijeka (HR), 2011, Chapter 4.

[29] G. Moek, E. Lutz, and W. Mosborg, *Risk Assessment of RNP1 and RVSM in the Southern Atlantic Flight Identification Regions,20833*, ARINC, Annapolis, 2001.

[30] International Civil Aviation Organization (ICAO), *International Standards and Recommended Practices, Annex 6, Operation of Aircraft (Tenth Edition)*, ICAO, Montréal, Canada, 2018.

[31] Convention on International Civil Aviation, *Doc 4444:Air Traffic Management*, Montréal INTERNATIONAL CIVIL AVIATION ORGANIZATION (ICAO), Montreal, 2016.